ANALYSIS OF AERODYNAMIC PERFORMANCE OF EROSION AIRFOIL WITH REYNOLDS NUMBER VARIATIONS

[1]James Julian, [2]Waridho Iskandar, [3]Fitri Wahyuni
[1,2,3]Fakultas Teknik Universitas Pembangunan Nasional Veteran Jakarta
Jl. Rs. Fatmawati, Pondok Labu, Jakarta Selatan, 12450, Indonesia
[1]zames@upnvj.ac.id, [2]waridho.iskandar@upnvj.ac.id, [3]fitriwahyuni@upnvj.ac.id

Abstrak

Erosi pada airfoil NACA 0015 diteliti dengan menggunakan metode komputasional untuk menyelidiki perubahan performa dari airfoil. NACA 0015 yang digunakan pada penelitian ini memiliki panjang chord 1 m, panjang chord ini kemudian digunakan sebagai paramter dalam menghitung bilangan Reynolds pada airfoil. Proses komputasi dilakukan dengan domain C dengan dimensi yang telah diatur sedmikian rupa untuk dapat menghindari pengaruh boundary terhdap hasil komputasi yang diperoleh pada penelitian ini. Governing equation untuk penelitian ini adalah RANS dimana didukung oleh model turbulensi standar k-ω. Erosi pada airfoil memiliki pengaruh yang sangat besar terhadap perubahan performa aerodinamika dari airfoil. Melalui sudut pandang C_l, erosi pada airfoil dapat menurunkan nilai C_l dari airfoil secara signifikan terutama pada AoA yang tinggi. Sebaliknya jika dilihat dari sudut pandang C_d erosi pada airfoil mengakibatkan adanya peningkatan nilai C_d. Peningkatan nilai C_l dapat dijelaskan dengan memvisulisasikan kontur tekanan di sekitar airfoil. Kontur tekanan menunjukkan adanya penurunan tekanan di lower namun terjadi peningkatan di upper. Sementara itu kontur kecepatan dan stremline dapat menjeskan adanya penyebab peningkatan C_d dimana dengan sangat jelas disebabkan oleh adanya separasi di area erosi dan di upper surface dari airfoil.

***Kata Kunci**: aerodinamika, erosi, komputasi, NACA 0015, Reynolds number*

Abstract

Erosion on airfoil was investigated using computational methods to investigate changes in the performance of the airfoil. NACA 0015 used in this study has a chord length of 1 m, which is then used as a parameter in calculating the Reynolds number. The computational process is carried out with domain C with dimensions that have been arranged in such a way as to avoid the influence of the boundary on the computational results obtained in this study. The governing equation for this study is RANS which the standard *k-ω* turbulence model supports. Erosion has a considerable influence on changes in the aerodynamic performance of the airfoil. Erosion can significantly reduce the C_l value of the airfoil, especially at high AoA. Erosion of the airfoil results in an increase in the value of C_d. The increase in C_l value can be explained by visualizing the pressure contour around the airfoil. The pressure contour shows a decrease in pressure in the lower but an increase in the upper. The velocity and streamline contours can explain the cause of the increase in C_d, which is very clearly caused by the separation in the erosion area and on the upper surface of the airfoil.

***Keywords**: aerodynamic, computation, erosion, NACA 0015, Reynolds number*

INTRODUCTION

Wind power plant is one of the energy sources currently being focused on and being developed to replace conventional power plants. Wind power plants, in general, are wind turbines. Wind turbines are divided into vertical-axis wind turbines (VAWT) and

horizontal-axis wind turbines (HAWT)[1]. Both types of wind turbines work by utilizing the blades. The wind turbine harnesses the wind's kinetic energy into motion energy in the wind turbine blades to rotate the shaft of geneartor[2]. Therefore, the capacity and energy conversion capability of a wind turbine is highly dependent on the performance of the blades. However, in its implementation, wind turbines have several challenges that must be faced. One of these challenges is damage to the structure of the wind turbine blades. Therefore, several studies have examined and studied the aerodynamic performance of wind turbine sections to obtain comprehensive information[3].

Broeren and Bragg conducted an experimental study to investigate the performance of intercycle ice accreations on various types of airfoils. The study was conducted on airfoils with NACA 23012, NACA 3415, and NLF 0414 stops. The Reynolds number was kept at 1.8×10^6, while the Mach number was kept at 0.18. In NACA 23012 airfoil, the maximum lift coefficient (C_l) for airfoils with an iced configuration is 0.65 to 0.8. It has decreased compared to a clean airfoil with a maximum C_l of 1.47. Meanwhile, in the NLF 0414 airfoil, there was a decrease in the maximum C_l, which was previously at a value of 1.34 to 0.9 to 1.05. Furthermore, the maximum NACA 3415 C_l airfoil decreased from 1.37 to 0.85 to 0.95[4]. Ge et al. studied the effect of defects on the airfoil's leading edge on wind turbines' power loss. The research specifically studied two types of defects in the airfoil. The two types of defects consist of surface-concaved deep and surface-distributed shallow defects. The research focuses on one type of airfoil, namely S809. The study was conducted using the CFD method. On a deep defect, a vortex forms in the defect cavity, affecting the momentum exchange between external and internal flows. At a high angle of attack, the fluid flow on the suction side is completely dominated by the fluid flow separation along the airfoil surface from the leading edge to the trailing edge. Meanwhile, in the shallow defect, the opening range and the defect's shape affect the airfoil's aerodynamic performance. However, the depth of the defect has the most significant influence. Specifically, in this study, there was a maximum decrease in C_l of 35% to 61%. It was followed by an increase in the drag coefficient of C_d in the range of 131% to 217% [5]. Gharali and Johnson also researched the same type of airfoil, namely S809. The research studies erosion on airfoils. The method used is also a computational method using Fluent 12.1 software. The research proposed two types of turbulence models: realizable k-ε and SST k-ω. Ultimately, the k-ω SST turbulence model was chosen because it was proven to predict stalls very well. Eroded airfoil causes a decrease in C_l and an increase in C_d, affecting the overall airfoil performance[6].

Overall, studies regarding airfoil damage have been carried out in the studies

above. The damage can be in defect, iced configuration, and erosion. The conclusions given from each study have also shown almost similar conclusions. From an aerodynamic perspective, airfoil damage has caused a decrease in the aerodynamic performance of the airfoil. Unfortunately, no research comprehensively examines the influence of the Reynolds number. It is necessary because wind turbines and other aerodynamic devices operate at various fluid speeds in actual conditions. This study aims to study the effect of changes in the Reynolds number on the aerodynamic performance of eroded airfoils. Besides that, the above studies are more focused on the S809 airfoil. Research on NACA airfoils is still not widely found, so there is a need for other studies that discuss other types of airfoils to be able to add to the data treasury. Therefore, in this study, the airfoil being analyzed was NACA 0015, which is widely applied to various devices such as wind turbines, airplanes, MAVs, and UAVs.

METHODOLOGY

Flowchart

The research process consists of several successive stages, as described in Figure 1. The earliest stage of the research is pre-processing. Pre-processing is divided into two parts, namely, creating geometry and meshing. Geometry is made using CAD software. The output of this activity is the airfoil geometry and its boundary conditions. Meshing is dividing the continuous domain into small or discrete parts. The research process can be continued with solving. The solving process is entirely carried out with a computer device. In this process, each discrete is calculated numerically to get computational results. If the solving process has been completed, it can be continued with data collection and fluid flow visualization. All data from research results are collected to proceed to the validation and verification stages. Visualization of fluid flow can be in the form of pressure contours, velocity contours, and fluid flow streamlines. This study conducted validation and verification tests to ensure the quality of the data obtained from the computational results. Validation is carried out by comparing the computational data obtained with experimental data. Verification in this study was carried out based on a mesh independence test. After the data is confirmed feasible, it can proceed to the data analysis stage.

Airfoil

Airfoil is a wing cross-sectional profile that can manipulate fluid flow to generate lift[7][8]. Generally, the airfoil consists of several parts, including the upper and lower surfaces[9]. In order to produce lift, the airfoil has a higher curvature on the top side than the bottom side. However, in some airfoils, one can find a condition where the upper and lower sides have the same curvature and opposite curvature directions. It is known as a

symmetrical airfoil. Symmetrical airfoils have several advantages over asymmetrical airfoils. The advantage lies in its stability when the airfoil is at a low angle of attack. Due to its stability, the symmetrical airfoil type is generally implemented in various aerodynamic devices that require stability and precise control. Among them are MAVs, UAVs, small airplanes, and wind turbines. In addition, this type of airfoil has also become easier to manufacture. One example of a symmetrical airfoil is NACA 0015, which will be used as an object of research. NACA 0015 geometry can be seen in Figure 2[10].

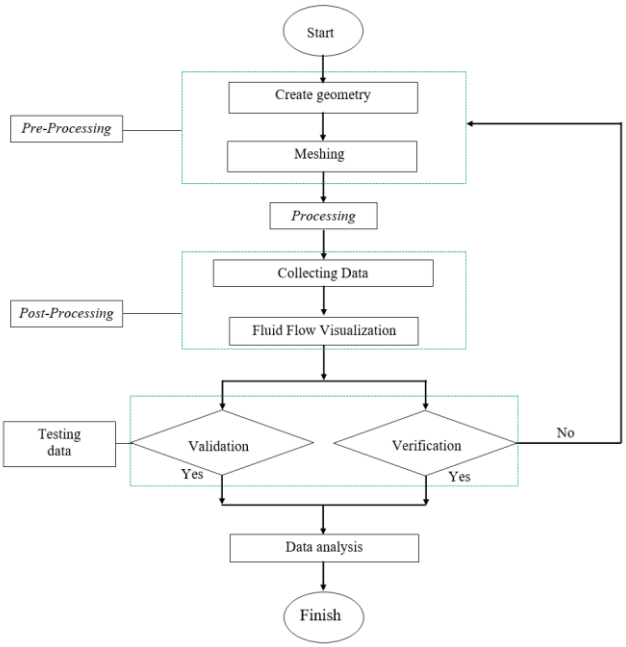

Figure 1. Flowchart

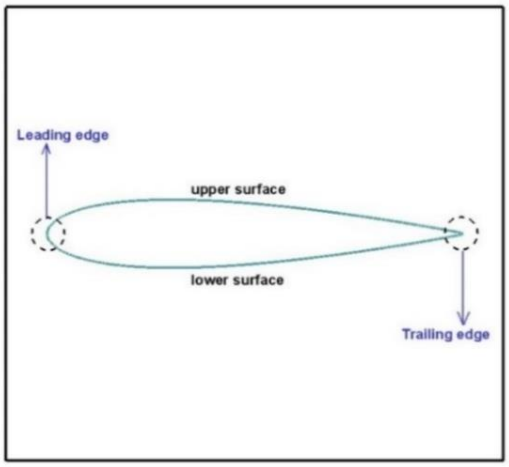

Figure 2. Airfoil

Computational methodology

The computational process uses steady flow, turbulence, and isothermal. The analysis was carried out by applying two-dimensional geometry. The type of fluid used is air with a speed corresponding to the Reynolds number. The Reynolds number is calculated using the chord length parameter of the airfoil, which is 1m. The boundary conditions used in this study are arranged in the same way as in the study conducted by Julian et al. 2022[11]. Further to the regulatory equation used in this study is the RANS equation. The RANS equation models turbulent fluid flow, where fluid motion cannot be predicted precisely using the basic Navier-Stokes equation[12]. The RANS equation assumes that the time average of fluid flow variables, such as velocity and pressure, are predictable and measurable. Therefore, the RANS equation makes obtaining a statistical average of the fluid flow possible[13]. The RANS equation consists of two main parts: the continuity equation, which describes the conservation of mass, as in equation 1, and the momentum equation, which describes the conservation of momentum, as in equation 2[14].

$$\frac{\partial \rho}{\partial t} + \frac{\partial}{\partial x_i}(\rho u_i) = 0 \tag{1}$$

$$\frac{\partial}{\partial t}(\rho u_i) + \frac{\partial}{\partial x_i}(\rho u_i u_j) = \frac{\partial p}{\partial x_i} + \frac{\partial}{\partial x_j}\left[\mu\left(\frac{\partial u_i}{\partial x_j} + \frac{\partial u_j}{\partial x_i} - \frac{2}{3}\delta_{ij}\frac{\partial u_i}{\partial x_i}\right)\right] + \frac{\partial}{\partial x_i}\left(-\rho\overline{u_i' u_j'}\right) \tag{2}$$

The turbulence model equation

A turbulent fluid flow always has very complicated fluctuation values. These fluctuations can be predicted using a turbulence model[15]. Thus, the turbulence model is an additional equation to complete the RANS equation. Furthermore, the turbulence model can be used in various fluid flow case studies such as aerodynamics, internal flow, and various chemical industry applications. In CFD, there are many turbulence models available. Several turbulence models have varying numbers of equations. Some turbulence models have two equations, such as standard *k-ε*, standard *k-ω*, Realizable *k-ε*, SST *k-ω*, and others. Several turbulence models have only one equation, such as Spalart-Allmaras. However, in this study, the turbulence model is the standard k-ω. The advantage of this turbulence model is that it can provide reasonable predictions at low Reynolds numbers. It can provide an advantage in this study considering the Reynolds numbers used are low Reynolds numbers, namely 10^5, 2.68×10^5, and 4.63×10^5. The mathematical equation for the standard k-ω turbulence model is in equations 3 and 4. Equation 3 represents the turbulent kinetic energy equation. Besides, equation 4 represents the specific dissipation rate[16].

$$\rho \frac{Dk}{Dt} = \tau_{ij} \frac{\partial \overline{u_i}}{\partial x_j} - \rho\beta^* f_{\beta^*} k\omega + \frac{\partial}{\partial x_j}\left[\left(\mu + \frac{\mu_t}{\sigma_k}\right)\frac{\partial k}{\partial x_j}\right] \quad (3)$$

$$\rho \frac{D\omega}{Dt} = \alpha \frac{\omega}{k} \tau_{ij} \frac{\partial \overline{u_i}}{\partial x_j} - \rho\beta f_\beta \omega^2 + \frac{\partial}{\partial x_j}\left[\left(\mu + \frac{\mu_t}{\sigma_\omega}\right)\frac{\partial \omega}{\partial x_j}\right] \quad (4)$$

Detail computation

The computations were performed using the NACA 0015 geometry with a chord size of 1m. The airfoil chord length is represented by the symbol C. A C-shaped domain surrounds the airfoil. This domain is composed of semi-circle and rectangular. The airfoil's trailing edge is placed at the center of the semi-circle. The dimensions of the semi-circle are 15c in radius, while the rectangle's dimensions are 20C and 30C. This dimension is good enough and feasible to avoid computational domain effects. In general, the computational domain is given in Figure 3[17]. Several computational parameters are given in Table 1. The properties table provides a more detailed description of computational details, such as the Reynolds number, AoA variations, and defined boundary conditions.

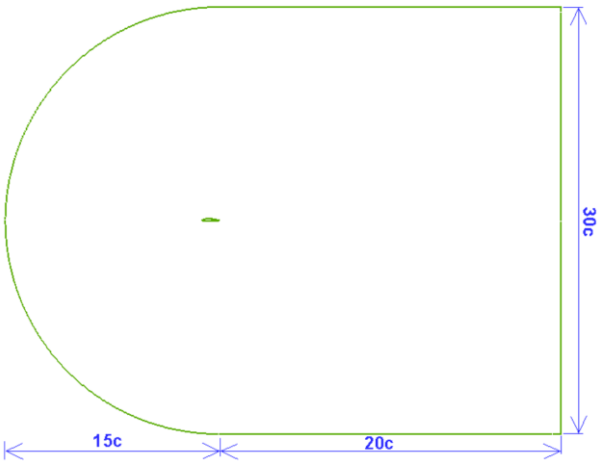

Figure 3. Computation domain

Tabel 1. Detail of paraleters in computation

Parameters	Definition
Reynolds number	10
AoA	0°-20°
inlet	Velocity inlet
outlet	Pressure outlet
airfoil	Wall-no slip

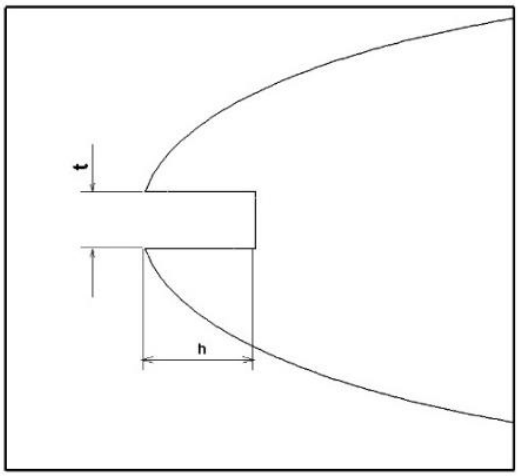

Figure 4. Erosion on the airfoil

Erosion on an airfoil

The actual use of airfoils in the field has several constraints that might hinder or even reduce their aerodynamic capabilities. One form of constraint experienced by the airfoil is the presence of erosion on the leading edge of the airfoil. Several types of erosion are commonly found on airfoils. These types of erosion can be seen in the research conducted by Gharali and Johnson. The erosion model discussed in this study is the B model. The dimensions of the erosion are expressed in the h and t variables. The h variable represents the erosion depth, while the t variable represents the erosion thickness. In general, the values of h and t are made non-dimensional; t is usually generalized by using a variable percentage of the thickness of the airfoil so that it becomes $t^*=t/t_{airfoil}$. The variable h is generalized using the chord length of the airfoil so that it becomes $h^*=h/c$. In this study, the value of $t^*=12\%$ and $h^*=4\%$. Erosion on NACA 0015 used in this study is given in Figure 4[6].

RESULTS AND DISCUSSION

Mesh independence test

Discussing the mesh independence test is an essential component in CFD simulation. The mesh independence test is a verification stage to test the feasibility of the number of elements used in the simulation. It is essential because the number of mesh elements can affect the simulation results. The mesh independence test must ensure that the number of mesh elements is feasible and that the simulation results will stay the same if the number of mesh elements is multiplied many times. The Richardson Extrapolation method developed by Roache is the mesh independence test method. The research was carried out with quadrilateral elements with a structured mesh type. The mesh independence test is carried out on a mesh with the number of elements 2×10^5, 10^5, and 5×10^4. Each stage of the mesh independence test is carried out with the same stages and processes as in the study conducted by Iskandar et al[18].

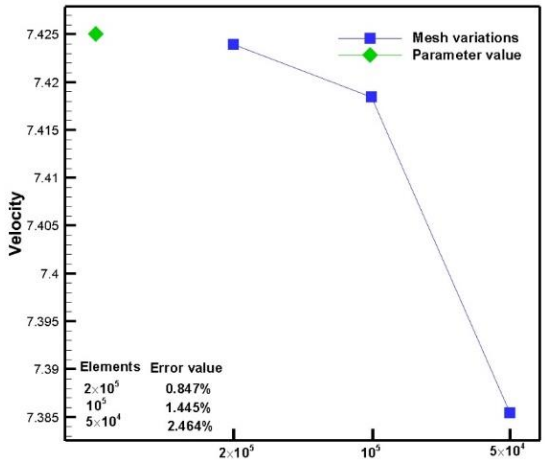

Figure 5. Mesh independence test

The Reynolds number for the mesh independence test is 10^5, where the baseline airfoil type is selected as the sample. Data collection for the mesh independence test is a variable velocity around the upper side of the airfoil. The results of the mesh independence test can be seen in Figure 5. Based on the mesh independence test results, it can be concluded that a mesh with elements of 2×10^5 gives the lowest error, so the entire simulation process is carried out using a mesh with a number of elements of 2×10^5.

Validation

The next step after mesh verification is to validate the computational results. Validation aims to compare data from computational results to those obtained through experimental results. Because this study only used computational methods, the experimental data was taken from another study that discussed the same object, namely NACA 0015[19]. The validation process was carried out under the same Reynolds number conditions, 4.63×10^5. The validation results are given in Figure 6a and Figure 6b. Figure 6a is the C_l data, while Figure 6b is the C_d data from the airfoil. The C_l data showed satisfactory results for almost all AoA. It shows the excellent ability of CFD to predict C_l airfoil data. Even so, there are still differences in the data obtained from the CFD results and experimental results. It can be seen from the stalled airfoil where the CFD results predict a 1° faster stall when compared to the experimental data. The C_d data also shows quite good results between the computational and simulation results, especially at AoA≤10°. At AoA> 10°, the simulation and experimental results show that there is a difference. Even so, this is still acceptable because at AoA> 10° the angle of attack of the airfoil is relatively high, and a vortex has formed, which makes fluid flow modeling very complex. This vortex has a considerable influence on the drag force, so the limitations of the vortex modeling also affect the prediction of C_d as a whole.

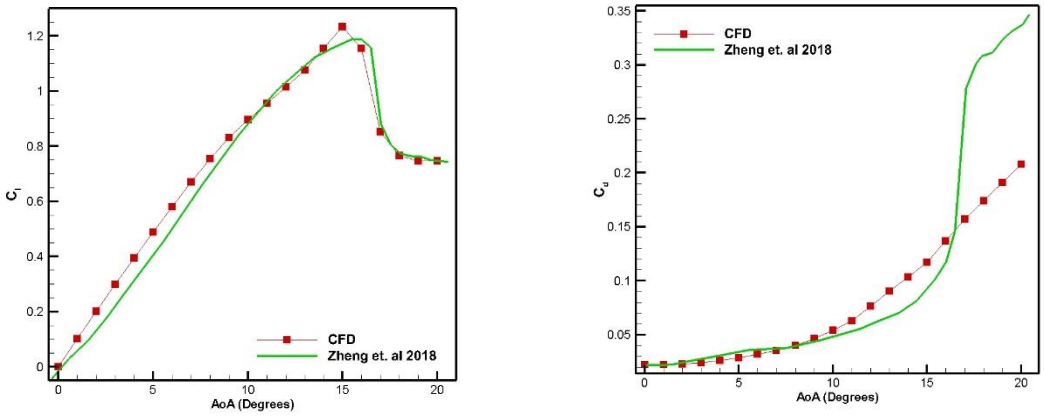

(a) (b)

Figure 6. Validation results (a) C_l (b) C_d

Analysis of the effect of erosion on the aerodynamic performance of NACA 0015

This study analyzes the aerodynamics of NACA 0015 with three variations of the Reynolds number. The first variation of the Reynolds number is 10^5, which shows the data for the baseline and airfoil conditions that have experienced erosion. The same thing was done for the second variation of the Reynolds number, 2.68×10^5, and the third variation of the Reynolds number, 4.63×10^5. In general, all variations of the Reynolds number show similar characteristics where at a very low AoA, the erosion effect does not significantly impact the C_l capacity of the airfoil. It can be seen in Figure 7a. Where AoA≤5°, the erosion effect has not been seen to reduce the value of C_l. The higher the AoA, the more pronounced the effects of erosion will be. It applies to all variations of the Reynolds number tested in this study. Furthermore, the eroded airfoil also experiences a faster stall. At a Reynolds number of 10^5, the previous baseline airfoil was at AoA=14°, while the airfoil that experienced erosion at the same Reynolds number stalled at AoA=9°. When the Reynolds number is 2.68×10^5, the airfoil also stalls at AoA=14°, while when it experiences erosion, it stalls at AoA=10°. When the Reynolds number of the airfoil is at 4.63×10^5, the stall is at AoA=16°; when the airfoil experiences erosion, the stall shifts faster to AoA=10°. Overall, it can be concluded that erosion on the airfoil is proven to reduce the C_l value of the airfoil. In addition, erosion of the airfoil also causes stall acceleration. This research proves that the erosion effect reduces the lift force of the airfoil.

Apart from C_l data, this study also discusses more aerodynamic data by analyzing C_d data. At Reynolds number 10^5 and AoA≤8°, the C_d value shows no significant change between the airfoil baseline and erosion. Then at 9°≤AoA≤15°, the increase in C_d becomes very extreme. Then at AoA≥16° the increase in C_d value on the airfoil is no longer as extreme as at 9°≤AoA≤15°. The same thing happened to the Reynolds numbers 2.68×10^5 and also 4.63×10^5. Overall, it can be concluded that erosion can worsen the aerodynamic

performance of the airfoil by increasing the C_d value. The cause of this increase in C_d value will be analyzed further using the contour data of fluid flow velocity and fluid pressure around the airfoil. C_d data on airfoils can be seen in Figure 7b.

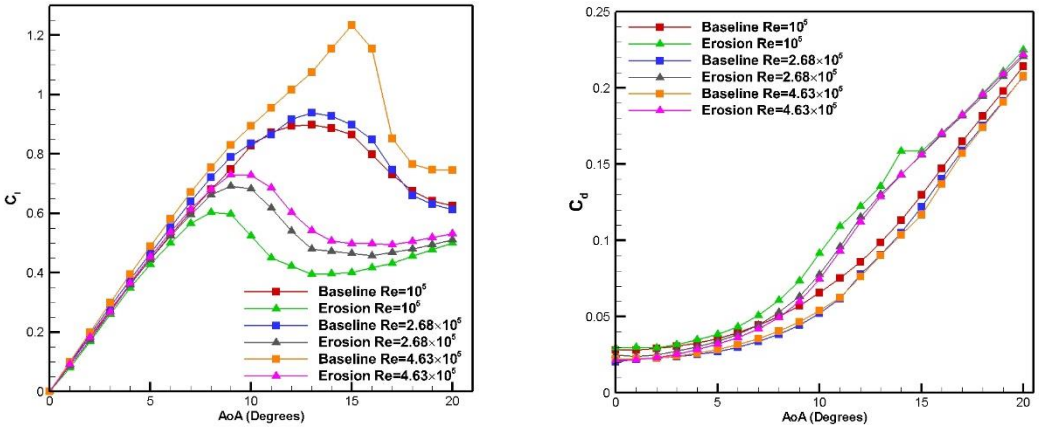

(a) (b)

Figure 7. Data of airfoil with erosion and without erosion (a) C_l and (b) C_d

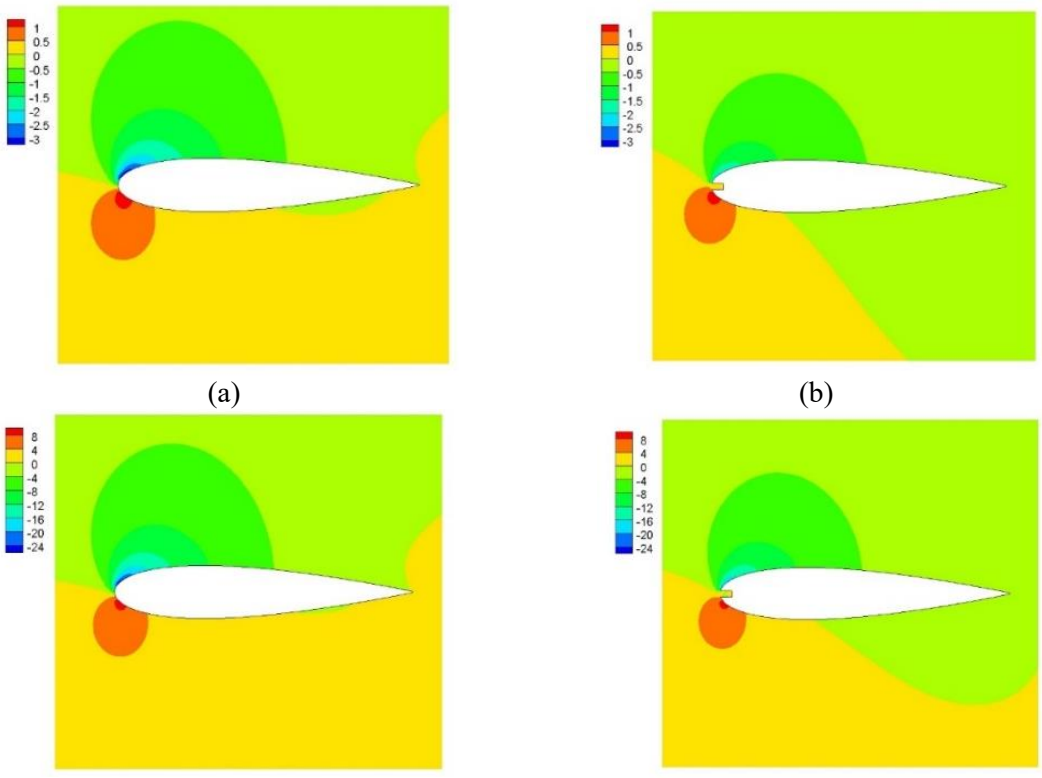

(a) (b)

(c) (d)

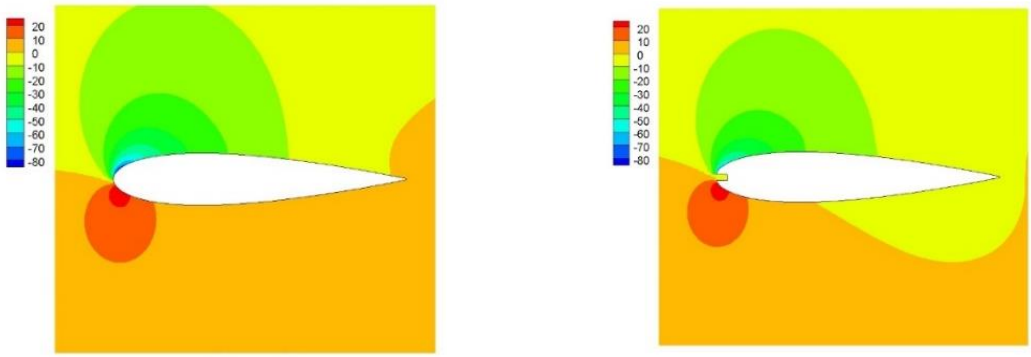

(d) (e)

Figure. 8. Pressure contour (a) without erosion in reynolds number 10^5 (b) with erosion in reynolds number 10^5 (c) airfoil without erosion in reynolds number 2.68×10^5 (d) airfoil with erosion in reynolds number 2.68×10^5 (e) airfoil without erosion in reynolds number 4.63×10^5 (f) airfoil with erosion in reynolds number 4.63×10^5

The contour of the fluid pressure flow through the airfoil is shown in detail in Figure 8. All variations of the Reynolds number are shown in this figure. However, the AoA used as the sample in this study was 10°. This AoA was chosen based on the previous discussion where the erosion of the airfoil has stalled at all variations of the Reynolds number. However, the baseline airfoil has not yet experienced a stall. When the Reynolds number is 10^5, the high-pressure area around the erosion experiences a pressure drop. However, this is not very visible when the Reynolds number of the airfoil is changed to 2.68×10^5 and 4.63×10^5. All variations of the Reynolds number the airfoil with erosion make the lower pressure area on the upper side smaller. Meanwhile, the pressure on the lower side experienced a decrease in pressure. It causes a decrease in C_l and an increase in C_d in the airfoil.

Furthermore, the fluid visualization is continued by discussing the velocity contour in the direction of the x-axis of fluid flow on the airfoil. In addition, the visualization is also equipped with a streamlined fluid flow. The AoA selected in this visualization is the same as in the pressure contour. Visualization using velocity contours in the direction of the x-axis aims to see the distribution of fluid velocity and observe the separation area on the back of the airfoil. This separation will be clearer if a streamlined fluid flow is given; a streamline will form recirculation when it enters the separated area. At the baseline airfoil, fluid flow recirculation has not been formed; this applies to all variations of the Reynolds number. Erosion causes a fluid flow separation; some eddies indicate recirculation in areas that experience erosion. Recirculation is also formed on the back of the airfoil when the Reynolds number is 10^5 and 2.68×10^5. The recirculation area will increase as the Reynolds number decreases. When the Reynolds number is 4.63×10^5, recirculation on the back of the airfoil will occur. Velocity contour and streamline on airfoil with and without erosion can be seen in Figure 9.

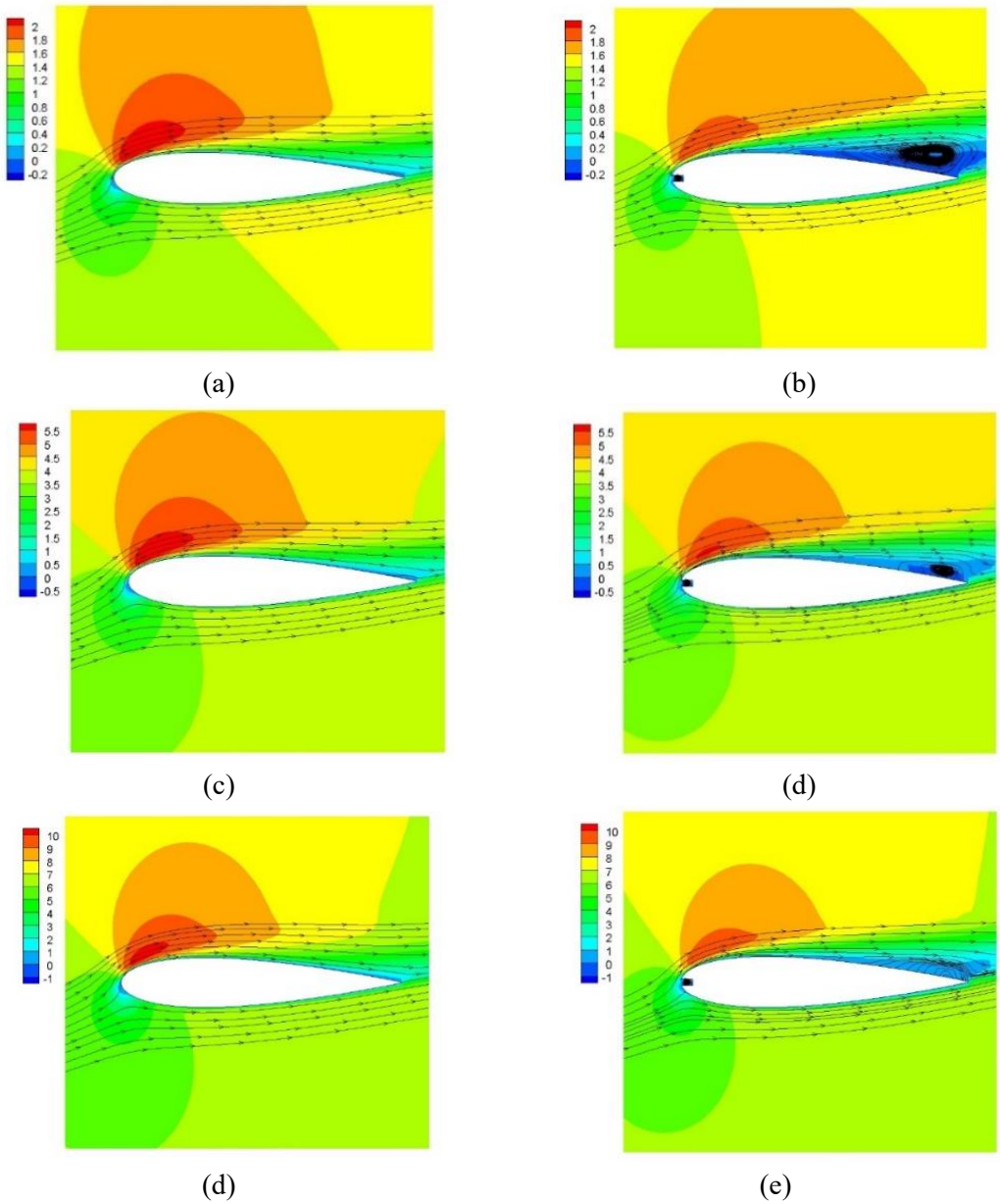

Figure. 9. Velocity contour (a) without erosion in reynolds number 10^5 (b) with erosion in reynolds number 10^5 (c) airfoil without erosion in reynolds number 2.68×10^5 (d) airfoil with erosion in reynolds number 2.68×10^5 (e) airfoil without erosion in reynolds number 4.63×10^5 (f) airfoil with erosion in reynolds number 4.63×10^5

CONCLUSION

Through a computational study, this research comprehensively analyzed the ability of an eroded airfoil. Specifically, the type of airfoil used is NACA 0015. There are three variations of the Reynolds number used, namely 10^5, 2.68×10^5, and 4.63×10^5. The research only used computational studies with the RANS equation and the standard *k-ω* turbulence model. The validation results show that all the computational setups have given quite good results when compared to the results obtained through experimental studies.

The C_l data shows a significant decrease when the airfoil is at AoA>5°. In addition, the erosion effect also makes the airfoil experience a faster stall. Besides that, erosion can also increase the ability of the airfoil to decrease by increasing C_d; this increase in C_d occurs in all AoA and all variations of the Reynolds number in the airfoil. Through the pressure contour data, it can be concluded that the cause of the decrease in C_l value is due to erosion, causing the pressure on the upper surface to increase and the pressure on the lower surface to decrease. Meanwhile, the velocity contours show that erosion results in fluid flow separation, while in the baseline airfoil, the separation does not occur at all variations of the Reynolds number. Separation of fluid flow can be found in areas of erosion and on the airfoil's upper surface. However, the separation of fluid flows on the upper surface varies depending on variations in the Reynolds number. The largest upper surface separation was found when the Reynolds number tested was 10^5; the size of the separation then became smaller when the Reynolds number increased to 2.68×10^5, and when the Reynolds number of the airfoil was increased again to 4.63×10^5 the separation was not fully formed.

REFERENCE

[1] E. Basta, M. Ghommem, L. Romdhane, and A. Abdelkefi, "Modeling and experimental comparative analysis on the performance of small-scale wind turbines," *Wind and Structures*, vol. 30, no. 3, pp. 261–273, 2020.

[2] J. Julian, W. Iskandar, and F. Wahyuni, "Leading edge modification of NACA 0015 and NACA 4415 inspired by beluga whale," *International Journal of Marine Engineering Innovation and Research*, vol. 8, no. 2, 2023.

[3] S. Rehman, M. M. Rafique, M. M. Alam, and L. M. Alhems, "Vertical axis wind turbine types, efficiencies, and structural stability-A Review," *Wind and Structures*, vol. 29, no. 1, pp. 15–32, 2019.

[4] A. P. Broeren and M. B. Bragg, "Effect of airfoil geometry on performance with simulated intercycle ice accretions," *J Aircr*, vol. 42, no. 1, pp. 121–130, 2005, doi: 10.2514/1.4734.

[5] M. Ge, H. Zhang, Y. Wu, and Y. Li, "Effects of leading edge defects on aerodynamic performance of the S809 airfoil," *Energy Convers Manag*, vol. 195, pp. 466–479, Sep. 2019, doi: 10.1016/j.enconman.2019.05.026.

[6] K. Gharali and D. A. Johnson, "Numerical modeling of an S809 airfoil under dynamic stall, erosion and high reduced frequencies," *Appl Energy*, vol. 93, pp. 45–52, 2012, doi: 10.1016/j.apenergy.2011.04.037.

[7] F. C. Megawanto, R. F. Karim, N. T. Bunga, and J. Julian, "Flow separation delay on NACA 4415 airfoil using plasma actuator effect," *International*

Review of Aerospace Engineering, vol. 12, no. 4, pp. 180–186, 2019.

[8] Harinaldi, M. D. Kesuma, R. Irwansyah, J. Julian, and A. Satyadharma, "Flow control with multi-DBD plasma actuator on a delta wing," *Evergreen*, vol. 7, no. 4, pp. 602–608, 2020, doi: 10.5109/4150513.

[9] F. C. Megawanto, Harinaldi, Budiarso, and J. Julian, "Numerical analysis of plasma actuator for drag reduction and lift enhancement on NACA 4415 airfoil," in *AIP Conference Proceedings*, AIP Publishing LLC, 2018, p. 050001.

[10] J. Zheng, Y. D. Cui, Z. Zhao, J. M. Li, and B. C. Khoo, "Flow separation control over a NACA 0015 airfoil using nanosecond-pulsed plasma actuator," *AIAA Journal*, vol. 56, no. 6, pp. 2220–2234, 2018, doi: 10.2514/1.J056111.

[11] J. Julian, W. Iskandar, F. Wahyuni, and F. Ferdyanto, "Computational fluid dynamics analysis based on the fluid flow separation point on the upper side of the NACA 0015 airfoil with the coefficient of friction," *Media Mesin: Majalah Teknik Mesin*, vol. 23, no. 2, pp. 70–82, 2022.

[12] J. Julian, F. Wahyuni, W. Iskandar, and R. Ramadhani, "The effect of curvature ratio towards the fluid flow characteristics in bend pipe based on numerical methods," *Turbo: Jurnal Program Studi Teknik Mesin*, vol. 12, no. 1, 2023.

[13] J. Julian, W. Iskandar, F. Wahyuni, and dan Nely Toding Bunga, "Aerodynamic performance improvement on NACA 4415 airfoil by using cavity," vol. 5, pp. 135–142, 2023.

[14] J. Julian, W. Iskandar, and F. Wahyuni, "Aerodynamics improvement of NACA 0015 by using co-flow jet," *International Journal of Marine Engineering Innovation and Research*, vol. 7, no. 4, Dec. 2022, doi: 10.12962/j25481479.v7i4.14898.

[15] W. Harinaldi, S. Adhika, and J. Julian, "The comparison of an analytical, experimental, and simulation approach for the average induced velocity of a dielectric barrier discharge (DBD)," in *The 10th International Meeting of Advances in Thermofluids (IMAT 2018): Smart City: Advances in Thermofluid Technology in Tropical Urban Development*, 2019, p. 020027.

[16] J. Julian, W. Iskandar, and F. Wahyuni, "Effect of single slat and double slat on aerodynamic performance of NACA 4415," 2022.

[17] J. Julian, W. Iskandar, F. Wahyuni, and N. T. Bunga, "Characterization of the co-flow jet effect as one of the flow control devices," *Jurnal Asiimetrik: Jurnal Ilmiah Rekayasa & Inovasi*, pp. 185–192, 2022.

[18] W. Iskandar, J. Julian, F. Wahyuni, F. Ferdyanto, H. K. Prabu, and F. Yulia, "Study of airfoil characteristics on NACA 4415 with reynolds number

variations," *International Review on Modelling and Simulations (IREMOS)*, vol. 15, no. 3, p. 162, Jun. 2022, doi: 10.15866/iremos.v15i3.21684.

[19] J. Zhang, K. Xu, Y. Yang, Y. Ren, P. Patel, and G. Zha, "Aircraft control surfaces using co-flow jet active flow control airfoil," in *2018 Applied Aerodynamics Conference*, in AIAA AVIATION Forum. American Institute of Aeronautics and Astronautics, 2018. doi: doi:10.2514/6.2018-3067.